Lateral Misalignment and Yaw Angle Control Considering Vehicle Dynamics Based on Receiving Energy in Dynamic Wireless Power Transfer

Tomoaki Koishi * **Binh-Minh Nguyen** * **Osamu Shimizu** *
Shota Yamada * **Hiroshi Fujimoto** *

* *The University of Tokyo 5-1-5, Kashiwanoha, Kashiwa, Chiba, 277-8561, Japan (e-mail: koishi.tomoaki21@ae.k.u-tokyo.ac.jp).*

Abstract: Recently, dynamic wireless power transfer (DWPT) has been shown to be a promising technology for the widespread of electric vehicles (EVs). To utilize this technology, a critical challenge is to eliminate the coil misalignments, which cause a decrease in the coupling coefficient, thereby considerably degrading the power transfer efficiency. Considering the rectangular coils, this paper presents a new method to estimate and eliminate lateral misalignments. Based on the dynamics model of the vehicle, the lateral misalignment is estimated by the fusion of the DWPT current and the onboard inertial measurement unit. On the other hand, the misalignment and the yaw angle of the vehicle are simultaneously controlled by using rear in-wheel motors and the front active steering system. The effectiveness of the proposed method has been demonstrated by both simulations and experiments using a vehicle developed by our research group.

Keywords: Positioning systems, Energy control in transportation, Motion control, Wireless power transfer, Parameter and state estimation

1. INTRODUCTION

Recently, electric vehicles (EVs) have been gaining attention due to growing concerns about environmental issues such as global warming and air pollution caused by exhaust gas. However, the long charging time and the short cruising distance have hindered the widespread of EVs. Dynamic wireless power transfer (DWPT) has been developed to address this problem [Covic and Boys (2013); Li and Mi (2015); Patil et al. (2017); Shimizu et al. (2020); Sumiya et al. (2021)]. Receiver coils are attached to EVs and run over transmitter coils embedded in the ground, which transfer electric power to EVs through magnetic resonance. Since rectangular coils have a longer charging area and less leakage electromagnetic field, they have been studied for DWPT. To realize the DWPT, it is necessary to deal with the efficiency reduction caused by a lateral misalignment between the transmitter and receiver coils. It is well known that the lateral misalignment degrades the coupling coefficient, thereby decreasing the power transfer efficiency.

Previous research has proposed methods to estimate lateral misalignment and eliminate it by positioning control. These methods do not need the additional primary side control, unlike the method proposed by Tavakoli and Pantic (2017). While there are image processing or GPS methods to estimate the vehicle position [Zheng and Li (2020); Rose et al. (2014)], methods using electrical parameters, such as voltage and current, have been gaining attention [Sukprasert et al. (2015); Hwang et al. (2017); Sithinamsuwan et al. (2020)]. The methods are superior

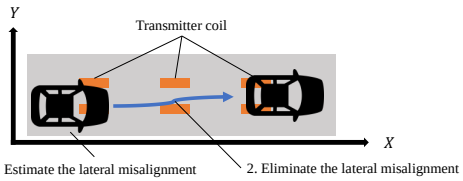

Fig. 1. Goal of this study: estimate and eliminate the lateral misalignment.

in that they do not use additional sensors to achieve the required accuracy and do not depend on the misalignment between the transmitter coil and the road marker. However, they aim at the DWPT system with circular coils or long charging lanes; hence, they cannot be applied to the system with rectangular coils.

Recently, by utilizing the DC link current on the receiver side, our research group has proposed a method to estimate and eliminate the lateral misalignment for the DWPT system with rectangular coils. The key idea of the method is to obtain a relationship between the lateral misalignment and the mean of the current. Then the approximation model of the relationship was derived, and the lateral misalignment can be calculated with high accuracy in real time. However, the effectiveness of the method was only evaluated using a test bench without vehicle dynamics.

The contribution of this paper is to further apply the method from the test bench to a real experimental vehicle. Figure. 1 shows the goal of this study. To support the drive, it is not enough to compensate only for the lateral misalignment as in the work of Sukprasert et al. (2015).

Table 1. PARAMETER DESCRIPTION

Parameter	Description
l_f, l_r	distance from c.g. to front and rear axles
C_f, C_r	tire cornering stiffness
m	vehicle mass
I_z	moment of inertia
r	wheel radius
d	tread of the rear axle
l_{cx}, l_{cy}	x- and y-axis distance from the center of gravity to the receiver coil
θ	yaw angle
γ	yaw rate
β	body sideslip angle
Y_{cg}	lateral position of the center of gravity
Y_{coil}	lateral misalignment between the transmitter and receiver coils
v	absolute velocity of the vehicle
v_x, v_y	x- and y-axis components of v
δ_f	front wheel steering angle
N_z	yaw moment generated by the in-wheel motors
T_{rr}, T_{rl}	torques of the left rear and right rear motors

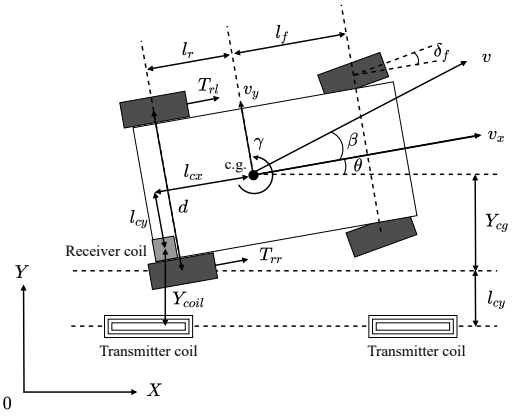

Fig. 2. Model of a vehicle with coil placements.

To simultaneously control the lateral misalignment and yaw angle, this paper shows a new method to fuse the DC link current measurement with the onboard inertial measurement unit (IMU). The method uses the vehicle dynamics model to estimate the lateral misalignment and the yaw angle from the outputs of the sensors. Furthermore, the lateral misalignment and the yaw angle are controlled by integrating the rear in-wheel-motors and the front active steering mechanisms. Numerical simulation shows that the lateral misalignment and the yaw angle can be successfully controlled. The proposed control system can improve the DWPT efficiency from 81.0 % in the first transfer to 94.2 % in the second transfer.

2. MODELING

2.1 Vehicle Dynamics Model

Figure. 2 describes a four-wheel vehicle model with the transmitter coil and the receiver coil attached to the rear wheel. In this study, the vehicle is driven by two rear in-wheel motors. Table 1 shows the parameter description. Since the in-wheel motors can control T_{rr} and T_{rl} independently, N_z is generated by the in-wheel motors, for instance $N_z = (T_{rr} - T_{rl})\,\frac{d}{2r}$.

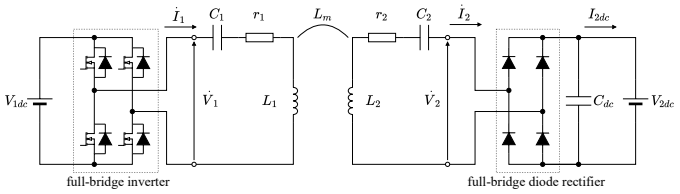

Fig. 3. Circuit diagram of WPT in this study.

Then, the equations of motion can be expressed as follows under the assumption that the tire forces are in the linear region:

$$\begin{aligned} mv_x(\dot{\beta}+\gamma) =& 2C_f\left(\delta_f - \frac{l_f}{v_x}\gamma - \beta\right) \\ &+ 2C_r\left(\frac{l_r}{v_x}\gamma - \beta\right), \\ I_z\dot{\gamma} =& 2l_fC_f\left(\delta_f - \frac{l_f}{v_x}\gamma - \beta\right) \\ &- 2l_rC_r\left(\frac{l_r}{v_x}\gamma - \beta\right) + N_z, \\ \dot{Y}_{cg} =& \frac{v_x}{\cos\beta}\sin(\beta+\theta) \simeq v_x(\beta+\theta), \\ \dot{\theta} =& \gamma. \end{aligned} \tag{1}$$

With respect to the placement of the receiver coil in Fig. 2, Y_{coil} can be derived as

$$Y_{coil} = Y_{cg} - (l_{cx}\sin\theta - l_{cy}(1-\cos\theta)). \tag{2}$$

2.2 Circuit Analysis

This study considers the WPT system shown in Fig. 3. A full-bridge inverter is used on the transmitter side, and a full-bridge diode rectifier is used on the receiver side. A constant voltage load is used to imitate a battery. V, I, r, L, and C denote the voltage, the current, the resistance, the self-inductance, and the capacitance, respectively. The subscripts '1', '2', and 'dc' indicate the transmitter side, the receiver side, and the rectified components, respectively.

The angular frequency of the supplied voltage ω_0 is set to satisfy the resonance conditions of both the transmitter and receiver sides.

The output voltage of the inverter V_1 is a square wave. However, the following analysis neglects the high-order harmonics since the WPT circuit functions as a bandpass filter. Since V_1 and V_2 are the RMS values, the following relationship can be derived from the Fourier series expansion:

$$V_1 = \frac{2\sqrt{2}}{\pi}V_{1dc},\ V_2 = \frac{2\sqrt{2}}{\pi}V_{2dc}. \tag{3}$$

Thus, the efficiency can be written as follows:

$$\eta = \frac{V_{2dc}(\omega_0 L_m V_{1dc} - R_1 V_{2dc})}{V_{1dc}(\omega_0 L_m V_{2dc} + R_2 V_{1dc})}, \tag{4}$$

where L_m denotes the mutual inductance between the transmitter and receiver coil.

Therefore, if the mutual inductance is positive, the mutual inductance and the efficiency have a positive correlation.

From (3), the receiver side DC current I_{2dc} can be approximated as follows:

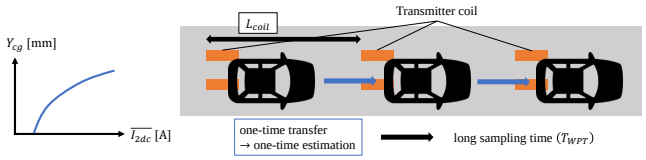

Fig. 4. The estimation results from DWPT information are obtained with a long interval.

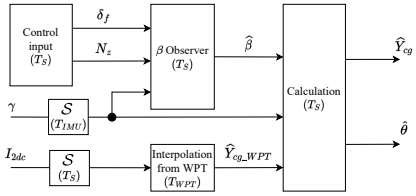

Fig. 5. Configuration of the proposed estimation method.

$$I_{2\mathrm{dc}} \simeq \frac{2\sqrt{2}}{\pi} I_2 = \frac{8}{\pi^2} \frac{\omega_0 L_m V_{1dc} - r_1 V_{2dc}}{\omega_0^2 L_m^2 + r_1 r_2}. \tag{5}$$

Therefore, if the DC link voltage of the transmitter and receiver sides are both constant, I_{2dc} depends only on the mutual inductance. Therefore, the mutual inductance can be obtained from I_{2dc}, which indicates that the lateral misalignment can be estimated from I_{2dc} since the mutual inductance depends on the lateral misalignment.

3. ESTIMATION AND POSITIONING CONTROL OF LATERAL MISALIGNMENT

3.1 Lateral position estimation using WPT information

Our research group has proposed a method to estimate lateral misalignment of the receiver coil from the mean of the DC link current in a one-time power transfer [Koishi et al. (2022)]. The method assumes that the parameters of the transmitter and receiver coils are given and uses the following approximation model using hyperbolic function and constants a, b, c:

$$Y_{coil} = \frac{1}{b} \operatorname{arccosh}\left(\frac{\overline{I_{2dc}} - c}{a}\right), \tag{6}$$

where $\overline{I_{2dc}}$ indicates the mean of the DC link current in the current-mean area, where the coupling coefficient is strong. The estimation error of this method is relatively large with a small misalignment. However, it does not affect the effectiveness since the mutual inductance is kept high with a small misalignment.

The estimation is performed once in a one-time transfer (Fig. 4). Concerning the common length of the transmitter coils, the distance between them, and the velocity of the vehicle in DWPT, the estimation result is obtained with an interval longer than that of the IMU T_{IMU}. For instance, if the distance between the transmitter coils is 3 m and the longitudinal velocity of the vehicle is 2 m/s, T_{WPT} is 1.5 s, and T_{IMU} is 1 ms by using the IMU unit AU7864 produced by Tamagawa Seiki Co., Ltd.

3.2 Estimation method

Fig. 5 shows the proposed estimation process. As described in the previous sub-section, WPT is a kind of accurate

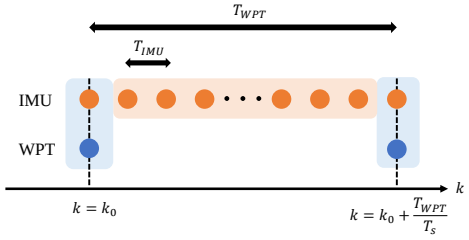

Fig. 6. Dual sampling of IMU and WPT.

sensor with a low-sampling rate. To deal with the long sampling time of WPT, it is possible to combine the long-sampling sensor with the short-sampling sensor, such as GPS and IMU [Nguyen et al. (2012)]. This study proposes the combination and estimation process. The initial value of yaw angle θ is assumed to be set to zero. The yaw rate γ can be obtained from IMU. From (1), the state space model can be written as follows:

$$\dot{x} = Ax + Bu,\ y = \gamma,$$
$$x = \begin{pmatrix} \beta \\ \gamma \end{pmatrix},\ u = \begin{pmatrix} \delta_f \\ N_z \end{pmatrix},$$

where each matrix is written as follows:

$$A = \begin{pmatrix} -\frac{2(C_f + C_r)}{m v_x} & -\frac{2(C_f l_f - C_r l_r)}{m v_x^2} - 1 \\ -\frac{2(C_f l_f - C_r l_r)}{I_z} & -\frac{2\left(C_f l_f^2 + C_r l_r^2\right)}{I_z v_x} \end{pmatrix},$$
$$B = \begin{pmatrix} \frac{2C_f}{m v_x} & 0 \\ -\frac{2C_f l_f}{I_z} & \frac{1}{I_z} \end{pmatrix}. \tag{7}$$

Then, the sideslip angle is estimated by the reduced order observer written as follows:

$$\dot{\hat{\beta}} = (A_{11} - LA_{21})\,\hat{\beta} + (A_{12} - LA_{21})\,\gamma + (B_{11} - LB_{21})\,\delta_f + (\beta_{12} - LB_{22})\,N_z + L\dot{\gamma},$$

where the subscripts 'ij' depict the i-row j-column component of the matrix, and L is the observer gain.

Let k be given as follows:

$$t = kT_S,$$

where T_S is the control period. In this paper, it is assumed that T_{IMU} equals to T_S. As explained in sub-section 3.1, the period T_{WPT} is much longer than T_{IMU} (Fig. 6). To estimate the lateral position with a high rate, the following algorithm is proposed using (1).

$$\hat{\theta}_k = \hat{\theta}_{k-1} + T_S \hat{\gamma}_{k-1},$$
$$\hat{Y}_{cg,k} = \begin{cases} \hat{Y}_{cg,k-1} + T_S v_x \left(\hat{\beta}_{k-1} + \hat{\theta}_{k-1}\right) & \left(k \neq k_0 + n\frac{T_{WPT}}{T_S}\right) \\ \hat{Y}_{cg\_WPT,k} & \left(k = k_0 + n\frac{T_{WPT}}{T_S}\right) \end{cases}, \tag{8}$$

where n is an integer, and $\hat{Y}_{cg\_WPT}$ is calculated from (2) and $\hat{Y}_{cg\_coil}$ in (6) as follows:

$$\hat{Y}_{cg\_WPT,k} = \hat{Y}_{cg\_coil,k} + \left(l_{cx} \sin\hat{\theta}_k - l_{cy}\left(1 - \cos\hat{\theta}_k\right)\right). \tag{9}$$

3.3 Control method

The proposed control system is shown in Fig. 7. Y_{cg}^* and θ^* are the command values of Y_{cg} and θ, and they are

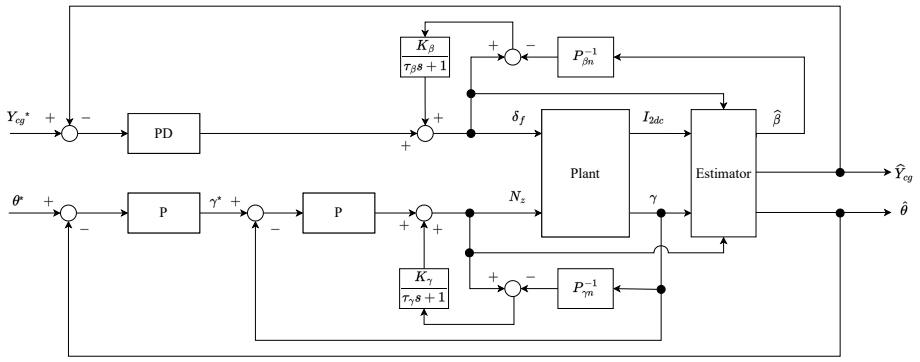

Fig. 7. Block diagram of positioning control.

both set to zero in this study. Lateral force observer (LFO) and yaw moment observer (YMO), which are proposed by Yamauchi and Fujimoto (2008) and Fujimoto et al. (2004), are used. LFO and the PD controller control the lateral position, and the yaw angle is controlled by YMO and the P controller of the yaw rate and the yaw angle. LFO and YMO are designed with the nominal model $P_{\beta n}(s)$ and $P_{\gamma n}(s)$. The stability of the overall system can be assured by selecting the controllers that stabilize the matrix of transfer functions from Y_{cg}^* and θ^* to $\hat{Y}_{cg}$ and $\hat{\theta}$. Due to the limitation of paper space, this discussion is not presented in this paper.

4. SIMULATION EVALUATION

4.1 Estimation

Simulations were performed for each case with one and multiple coils to evaluate the proposed estimation method. The simulations were performed by MATLAB/Simulink. The four-wheel model was established using the parameters of our experimental vehicle FPEV5 and used to simulate the vehicle dynamics. The DC link current was given by an approximation model of the AC current of the receiver coil proposed by Sithinamsuwan et al. (2020).

The human driver model described by Sharp et al. (2000) was used to control the vehicle. The controller model is described as follows:

$$\delta_f = -k_p e^{-s\tau} \left(Y_{cg} + L \sin\theta \right),$$

where k_p is the P gain, τ is the delay, and L is the distance from the center of gravity to the preview point. The initial lateral misalignment was 80 mm, and the initial yaw angle was set to zero. The first transmitter coil was placed at $x = 2\,\mathrm{m}$.

Table 2 shows the parameters used in the simulation. The white noise was added to the inputs δ_f, N_z, and the outputs a_y, γ. In this simulation, the vehicle speed is assumed to be constant ($v_x = 2\,\mathrm{m/s}$). The poles of the observer are selected as 50 rad/s.

Figure. 8 shows the simulation result. Blue lines of Y_{cg}, and θ show the actual values, and red lines show the estimated values. Y_{cg} is estimated with a small estimation error, as shown in Fig. 8(a). The noises of the inputs and the outputs were summed by the estimation process and accumulated in an area without the transmitter coils, which directly resulted in the errors of Y_{cg}.

Table 2. PARAMETERS OF SIMULATION

Parameter	Value
$\{l_f,\, l_r\}$	$\{1.11\,\mathrm{m},\, 1.44\,\mathrm{m}\}$
m	1100 kg
I_z	$840\,\mathrm{kg\,m^2}$
$\{l_{cx},\, l_{cy}\}$	$\{1.44\,\mathrm{m},\, 0.43\,\mathrm{m}\}$
v_x	2 m/s
$\{R_1,\, R_2\}$	$\{342.5\,\mathrm{m\Omega},\, 385.3\,\mathrm{m\Omega}\}$
$\{V_{1dc},\, V_{2dc}\}$	$\{100\,\mathrm{V},\, 100\,\mathrm{V}\}$
f_0	85 kHz

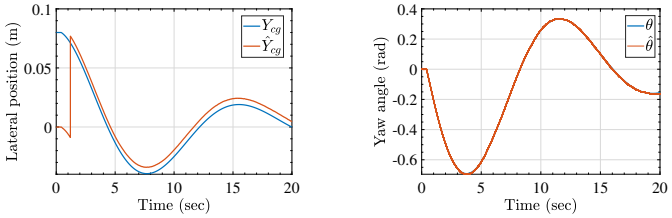

(a) Y_{cg} (b) θ

Fig. 8. Simulation result of the proposed estimation method with one coil.

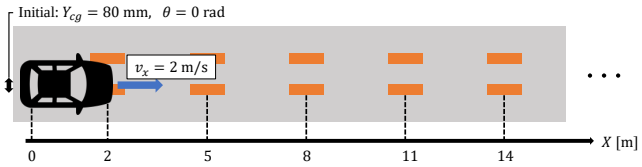

Fig. 9. Simulation setting of the overall control system.

As demonstrated above, the simulation result showed the effectiveness of the proposed estimation method.

4.2 Overall control system

A simulation was performed with multiple transmitter coils to evaluate the proposed control method. Figure. 9 shows the assumed condition of the simulation. The initial lateral misalignment was 80 mm, and the initial yaw angle was set to zero. The first transmitter coil was placed at $x = 2\,\mathrm{m}$, and the following coils were placed with the interval of 3 m. Table 3 shows the parameters of the controller. δ_f and N_z were input by the controller to control Y_{cg} and θ. The other conditions were the same as the simulation of the estimation method.

Table 3. PARAMETERS OF CONTROLLER

Parameter	Value
P gain of the PD controller of Y_{cg}	$0.568\,\mathrm{rad\,s\,m^{-1}}$
D gain of the PD controller of Y_{cg}	$0.217\,\mathrm{rad\,s^2\,m^{-1}}$
P gain of the P controller of θ	$0.5\,\mathrm{s^{-1}}$
P gain of the P controller of γ	$1.68 \times 10^3\,\mathrm{N\,m\,s}$
$\{K_\beta,\, K_\gamma\}$	$\{0.5,\, 0.9\}$
$\{\omega_\beta,\, \omega_\gamma\}$	$\{20\,\mathrm{rad/s},\, 20\,\mathrm{rad/s}\}$

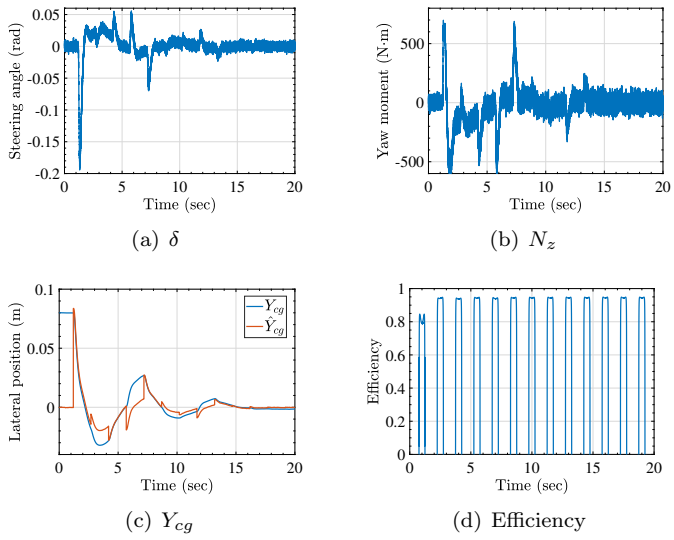

(a) δ (b) N_z

(c) Y_{cg} (d) Efficiency

Fig. 10. Simulation result of the proposed control method.

To evaluate the effectiveness of the proposed control method, the energy efficiency η_e of the first and second transfer was calculated as follows:

$$\eta_e = \frac{W_2}{W_1},$$

where W_1 is the output energy of the source in the current-mean area, and W_2 is the energy consumption of the load in the current-mean area.

Figure. 10 shows the simulation result. Y_{cg} and θ were controlled to zero, faster than the human driver model, as shown in Fig. 8. The RMSD of Y_{cg} was 24 mm with the proposed method, while 31 mm with the human driver model. The tracking error of Y_{cg} is thought to be due to the error from the estimation method from WPT. Moreover, as shown in Fig. 10(d), the energy efficiency was improved from 81.0 % in the first transfer to 94.2 % in the second transfer. This efficiency was stably maintained until the end of the simulation test.

As demonstrated above, the simulation result showed the effectiveness of the proposed overall control system.

5. EXPERIMENT

5.1 Setup

An experiment was conducted to verify the proposed estimation method. The experiment was performed using the experimental vehicle FPEV5, shown in Fig. 11. The vehicle is equipped with active front steering and two rear in-wheel motors. One transmitter coil was placed, and the vehicle ran over the coil. In the experiment, v_x will be controlled by the PI controller to be the constant velocity

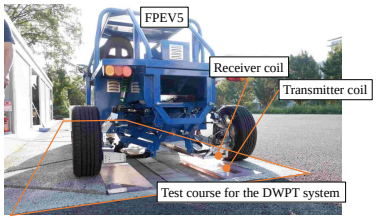

Fig. 11. Experimental vehicle FPEV5.

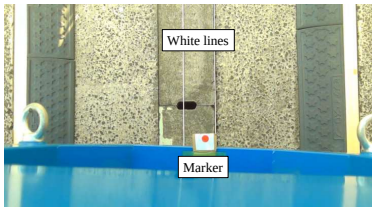

Fig. 12. Image obtained by the camera. The distance between the marker and the left white line was measured by image processing.

0.28 m/s. The vehicle position will be estimated by the proposed method and by image processing of the video obtained by a camera mounted on the rear of the vehicle. The image shows a marker mounted directly below the camera and a white line on the road surface as shown in Fig. 12, and the distance between the center of the marker and the white line is measured by image processing to estimate the lateral misalignment.

Two test cases were conducted. In case 1, the steering angle was set to eliminate the lateral misalignment, while the steering angle was constant in case 2.

5.2 Result and discussion

The experiment results are shown in Fig. 13 and Fig. 14. The blue lines in Fig. 13(c) and Fig. 14(c) show the lateral misalignment estimated by the proposed method, and the orange lines show the misalignment estimated by image processing. Broken lines show the estimated lateral misalignment before the WPT update.

In both cases, the lateral misalignment was estimated by WPT (at 2.5 s in case 1 and 3.0 s in case 2). The RMSD of the estimation after the WPT update was 12.7 mm in case 1 and was 7.4 mm in case 2. When the WPT information is available, the estimation error is less than 10 mm, which is relatively good in comparison with the RTK-GPS. In case 1, however, the estimation error increased as time passed. The error can be caused by the drift of the yaw rate from IMU and the model error. It is expected that the estimation from WPT will improve the accuracy with multiple coils, as shown in the simulation.

6. CONCLUSION

Based on the fusion of WPT and IMU, this paper proposes a new method for estimating and controlling the lateral misalignment and yaw angle of electric vehicles. The overall control system uses LFO and the PD controller to control Y_{cg}, and YMO and the P controller of θ and the yaw rate γ. The simulation was performed with one transmitter coil to evaluate the proposed estimation method, and

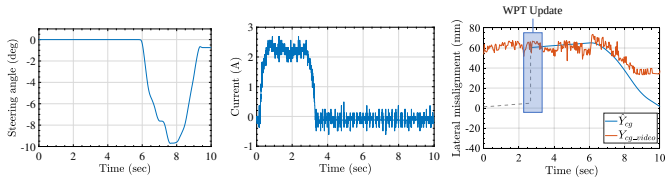

(a) δ (b) I_{2dc} (c) Y_{cg}

Fig. 13. Experiment result of the proposed estimation method in case 1.

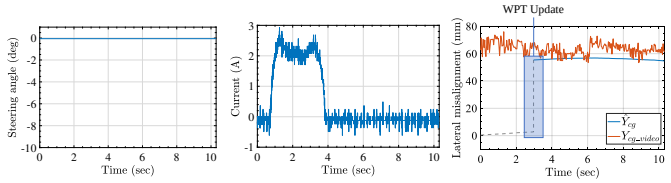

(a) δ (b) I_{2dc} (c) Y_{cg}

Fig. 14. Experiment result of the proposed estimation method in case 2.

the estimation method could successfully estimate Y_{cg} and θ. Another simulation was performed with multiple transmitter coils to evaluate the proposed overall control system. It was shown that the overall control system could control Y_{cg} and θ faster than the human driver model, and then the DWPT efficiency was improved from 81.0 % in the first transfer to 94.2 % in the second transfer. Furthermore, the experiment was conducted to verify the proposed estimation method, which showed effectiveness. In the future, experiments of the overall control system will be verified at a higher speed.

ACKNOWLEDGEMENTS

This work was partly supported by JST-Mirai Program Grant Number JPMJMI21E2, Japan, by Industrial Technology Research Grant Program from New Energy and Industrial Technology Development Organization (NEDO) of Japan (number 05A48701d), and by the Ministry of Education, Culture, Sports, Science and Technology grant (number 22246057 and 26249061).

REFERENCES

Covic, G.A. and Boys, J.T. (2013). Modern trends in inductive power transfer for transportation applications. *IEEE Journal of Emerging and Selected Topics in Power Electronics*, 1(1), 28–41. doi:10.1109/JESTPE.2013.2264473.

Fujimoto, H., Saito, T., and Noguchi, T. (2004). Motion stabilization control of electric vehicle under snowy conditions based on yaw-moment observer. In *The 8th IEEE International Workshop on Advanced Motion Control, 2004. AMC '04.*, 35–40. doi:10.1109/AMC.2004.1297637.

Hwang, K., Cho, J., Kim, D., Park, J., Kwon, J.H., Kwak, S.I., Park, H.H., and Ahn, S. (2017). An autonomous coil alignment system for the dynamic wireless charging of electric vehicles to minimize lateral misalignment. *Energies*, 10(3). doi:10.3390/en10030315.

Koishi, T., Matsumoto, R., and Fujimoto, H. (2022). Estimation and positioning control of lateral displacement using coil current in dynamic wireless power transfer with rectangular coil on dynamic bench. In *2022 Wireless Power Week (WPW)*, 322–326. doi:10.1109/WPW54272.2022.9854011.

Li, S. and Mi, C.C. (2015). Wireless Power Transfer for Electric Vehicle Applications. *IEEE Journal of Emerging and Selected Topics in Power Electronics*, 3(1), 4–17.

Nguyen, B.M., Wang, Y., Fujimoto, H., and Hori, Y. (2012). Sideslip angle estimation using gps and disturbance accommodating multi-rate kalman filter for electric vehicle stability control. In *2012 IEEE Vehicle Power and Propulsion Conference*, 1323–1328. doi:10.1109/VPPC.2012.6422741.

Patil, D., McDonough, M.K., Miller, J.M., Fahimi, B., and Balsara, P.T. (2017). Wireless Power Transfer for Vehicular Applications: Overview and Challenges. *IEEE Transactions on Transportation Electrification*, 4(1), 3–37. doi:10.1109/TTE.2017.2780627.

Rose, C., Britt, J., Allen, J., and Bevly, D. (2014). An integrated vehicle navigation system utilizing lane-detection and lateral position estimation systems in difficult environments for GPS. *IEEE Transactions on Intelligent Transportation Systems*, 15(6), 2615–2629. doi:10.1109/TITS.2014.2321108.

Sharp, R., Casanova, D., and Symonds, P. (2000). A mathematical model for driver steering control, with design, tuning and performance results. *Vehicle System Dynamics*, 33(5), 289–326. doi:10.1076/0042-3114(200005)33:5;1-Q;FT289.

Shimizu, O., Nagai, S., Fujita, T., and Fujimoto, H. (2020). Potential for co2 reduction by dynamic wireless power transfer for passenger vehicles in japan. *Energies*, 13(13). doi:10.3390/en13133342. URL `https://www.mdpi.com/1996-1073/13/13/3342`.

Sithinamsuwan, J., Fujimoto, H., and Hori, Y. (2020). Sensorless vehicle position detection in electric vehicle by logistic estimation function of mutual inductance. In *2020 IEEE PELS Workshop on Emerging Technologies: Wireless Power Transfer, WoW*, 254–259. doi:10.1109/WoW47795.2020.9291315.

Sukprasert, P., Nguyen, B.M., and Fujimoto, H. (2015). Estimation and control of lateral displacement of electric vehicle using WPT information. In *Proceedings - 2015 IEEE International Conference on Mechatronics, ICM*, 329–334. doi:10.1109/ICMECH.2015.7083997.

Sumiya, H., Takahashi, E., Yamaguchi, N., Tani, K., Nagai, S., Fujita, T., and Fujimoto, H. (2021). Coil scaling law of wireless power transfer systems for electromagnetic field leakage evaluation for electric vehicles. *IEEJ Journal of Industry Applications*, 10(5), 589–597. doi:10.1541/ieejjia.20009270.

Tavakoli, R. and Pantic, Z. (2017). Ann-based algorithm for estimation and compensation of lateral misalignment in dynamic wireless power transfer systems for ev charging. In *2017 IEEE Energy Conversion Congress and Exposition (ECCE)*, 2602–2609. doi:10.1109/ECCE.2017.8096493.

Yamauchi, Y. and Fujimoto, H. (2008). Proposal of lateral force observer with active steering for electric vehicle. In *2008 SICE Annual Conference*, 788–793. doi:10.1109/SICE.2008.4654763.

Zheng, Z. and Li, X. (2020). A novel vehicle lateral positioning methodology based on the integrated deep neural network. *Expert Systems with Applications*, 142. doi:10.1016/j.eswa.2019.112991.